Journal of Power Sources 195 (2010) 1888–1894

Contents lists available at ScienceDirect

Journal of Power Sources

journal homepage: www.elsevier.com/locate/jpowsour

In situ accelerated degradation of gas diffusion layer in proton exchange membrane fuel cell
Part I: Effect of elevated temperature and flow rate

Jinfeng Wu [a], Jonathan J. Martin [a], Francesco P. Orfino [b], Haijiang Wang [a,*], Colleen Legzdins [b], Xiao-Zi Yuan [a], Colin Sun [a]

[a] Institute for Fuel Cell Innovation, National Research Council Canada, 4250 Wesbrook Mall, Vancouver, B.C., Canada V6T 1W5
[b] Ballard Power Systems, 9000 Glenlyon Parkway, Burnaby, B.C., Canada V5J 5J8

ARTICLE INFO

Article history:
Received 11 September 2009
Received in revised form 10 October 2009
Accepted 12 October 2009
Available online 20 October 2009

Keywords:
Proton exchange membrane fuel cell
Gas diffusion layer
Barrier
In situ
Degradation mechanism
Material loss

ABSTRACT

Past studies have shown that both the substrate and microporous layer of the gas diffusion layer (GDL) significantly affect water balance and performance of a proton exchange membrane (PEM) fuel cell. However, little effort has been made to investigate the importance of GDL properties on the durability of PEM fuel cells. In this study, the in situ degradation behaviour of a commercial GDL carbon fiber paper with MPL was investigated under a combination of elevated temperature and elevated flow rate conditions. To avoid the possible impact of the catalyst layer during degradation test, different barriers without catalyst were utilized individually to isolate the anode and cathode GDLs. Three different barriers were evaluated on their ability to isolate GDL degradation and their similarity to a fuel cell environment, and finally a novel Nafion/MPL/polyimide barrier was chosen. Characterization of the degraded GDL samples was conducted through the use of various diagnostic methods, including through-plane electrical resistivity measurements, mercury porosimetry, relative humidity sensitivity, and single-cell performance curves. Noticeable decreases in electrical resistivity and the hydrophobic properties were detected for the degraded GDL samples. The experimental results suggested that material loss plays an important role in GDL degradation mechanisms, while excessive mechanical stress prior to degradation weakens the GDL structure and changes its physical property, which consequently accelerates the material loss of the GDL during aging.

1. Introduction

The gas diffusion layer (GDL) is typically a dual-layer carbon-based porous material, including a hydrophobic-treated carbon fiber paper or carbon cloth substrate covered by a thinner microporous layer (MPL) consisting of carbon black powder and a hydrophobic agent. Past studies have shown that the properties of both the GDL substrate and MPL play a significant role in water balance and performance of proton exchange membrane (PEM) fuel cells [1–6]. In these studies of GDLs, the impact of GDL materials and design on PEM fuel cell performance losses, rather than durability, has been the focal point. However, decreased GDL surface hydrophobicity has been clearly observed after 11,000 h of operation [7] and cold start conditions [8], unquestionably indicating that further investigation of the GDL is warranted. As the fuel cell operates, the polytetrafluoroethylene (PTFE) and carbon particles from the MPL of the GDLs are susceptible to chemical attack (i.e., $OH^{\bullet}$ radical as electrochemical by-product) and electrochemical (voltage) oxidation [9]. The loss of PTFE and carbon results in changes in the physical properties of the GDL, such as the decrease of conductivity and hydrophobicity, which further lowers MEA performance and negatively affects the durability of the whole fuel cell. So far, only a limited number of studies have focused on the degradation mechanisms of GDLs or on the relationship between GDL properties and fuel cell performance decay. Moreover, these publications have utilized mainly ex situ methods in the study of GDL durability to avoid the possible confounding effects from adjoining components such as the catalyst layer and bipolar plate.

The experiments of Borup et al. [10] showed that the loss of GDL hydrophobicity increased with operating temperature and when sparging air was used instead of nitrogen. Specifically, they ascribed the changes in GDL properties primarily to the MPL. Frisk et al. [9] aged GDLs by submerging the samples in 15 wt.% hydrogen peroxide at 82 °C. They found that weight loss and the reduction in MPL contact angle increased with the time of exposure and the increases were attributed to oxidation of the carbon in the MPL.

* Corresponding author. Tel.: +1 604 221 3038; fax: +1 604 221 3001.
E-mail address: haijiang.wang@nrc-cnrc.gc.ca (H. Wang).

0378-7753/$ – see front matter.
doi:10.1016/j.jpowsour.2009.10.022

Kangasniemi et al. [11] demonstrated the effect of electrochemical surface oxidation on GDL properties and found that the contact angle of the MPL surface decreased remarkably over time when the GDL samples were immersed in 1 M H_2SO_4 under potentiostatic treatment of 1.2 V vs. standard hydrogen electrode. Lee and Mérida [12] recently investigated GDL compressive strain under steady state (over 1500 h aging time at 80 °C and 200 psi) and freezing (54 freeze–thaw cycles between −35 and 20 °C) conditions. The changes in the aged GDL properties, such as electrical resistivity, bending stiffness, air permeability, surface contact angle, porosity, and water vapour diffusion were comprehensively studied. A maximum strain of 0.98% was measured over 1500 h of aging time and their further experiments showed that temperature had a larger effect on maximum strain than fixture load. Water phase transition during 54 freeze–thaw cycles had no effect on GDL strain but an increase in in-plane and through-plane air permeability (18 and 80%, respectively) was found, which was attributed to material loss during permeability measurements as a consequence of weakened MPL structure under freezing conditions. Most recently, Schulze et al. [13] found that the decomposition of PTFE in the electrodes induced a performance loss approximately twice as high as those related to the agglomeration of the platinum catalyst after 1000 h of fuel cell operation. However, the effect of PTFE degradation in the catalyst layer and GDL was not separated and the decomposition mechanism of PTFE was not thoroughly discussed in their paper.

The multi-faceted functions of the GDL in a PEM fuel cell include electron conduction, reactants distribution, water transport, heat conduction and mechanical support to the catalyst layer. The excessive mechanical, chemical/electrochemical and thermal stressors will undoubtedly affect the degradation of the GDL, and consequently bring down the durability of the whole fuel cell system. In this paper, the in situ degradation behaviour of the TORAY® TGPH-060 carbon fiber paper with MPL was investigated under elevated temperature and elevated flow rate. The effect of electrochemical stressor of elevated dynamic potentials on GDL degradation has also been investigated and the results will be disclosed in another paper. In order to avoid the impact of the adjoining catalyst layer, instead of CCM, different barriers without catalyst were tested and sandwiched individually between the anode and cathode GDLs during the degradation test. Three barriers were explored, including a Nafion® membrane, a Nafion® membrane covered with a perforated polyimide film and Nafion® coated with sacrificial MPLs on both sides and a polyimide border and finally, the last barrier was chosen for the GDL degradation studies. The changes in the GDL sample's properties over time were characterized, including through-plane resistivity, porosity, RH sensitivity as well as single-cell performance. Based on the experimental results, the degradation mechanisms of unstressed GDL and GDLs mechanically stressed prior to aging were explored.

2. Experimental

2.1. Experimental setup

The in situ GDL accelerated degradation experiment was performed with Tandem® TP50 fuel cell stack hardware (Tandem Tech. Ltd., Canada) on a Fuelcon® test station (500W Evaluator Test Station, Fuelcon Inc., Germany). For the Tandem® TP50 stack, the active area of each single cell was 50 cm^2 with a single serpentine channel for the anode flow field and dual parallel serpentine channels for the cathode flow field. A 3-cell TP50 stack was used to simultaneously age the following three different sets of GDL samples, i.e., as-received GDLs, hot-press stressed GDLs and assembly stressed GDLs. 6% PTFE-treated TORAY® TGPH-060 carbon fiber paper (190 μm thick) was utilized as both anode and cathode GDL substrate. The MPL ink, which consisted of acetylene black (Shawinigan AB50 grade; Chevron) and PTFE, was screen printed on the substrate. The carbon loading in both the anode and cathode MPL was kept at 10.0 mg cm^{-2}, while the PTFE contents in the anode and cathode MPLs were controlled at 10 and 20 wt.%, respectively. According to the available literature, the ideal operational conditions for PEM fuel cells include a temperature of about 80 °C and relatively low stiochiometry of approximate 2 and 3 for hydrogen and air, respectively [14–16]. To accelerate the GDL degradation, in this study GDL samples were subjected to a combination of elevated temperature and elevated flow rate continuously over 200 h. The hydrogen and air were first fully humidified at 80 °C then heated to 120 °C prior to their delivery to fuel cell stack. Deionised water was supposed to be utilized as coolant to control the fuel cell stack temperature, while here no coolant was employed in order to degrade GDL samples at elevated temperature beyond 100 °C. In the accelerated degradation test, the flow rate for hydrogen and air was controlled at 7.88 and 31.0 SLPM (standard liter per minute), respectively. The flow rates corresponded to relatively high theoretical stoichiometries of 7.5 and 11.8 at the anode and cathode, respectively, at a current density of 1 A cm^{-2}. The stack assembly was compressed with a bladder pressure of 100 psig and leak testing was performed before degradation testing.

In addition to as-received GDLs, other two sets of hot-press stressed and assembly stressed GDL samples were aged at the same time in order to explore the effects due to thermal and mechanical stresses encountered during manufacturing and/or operating processes such as hot-pressing process to prepare MEA and high-temperature PEM fuel cells operated above 100 °C. The conditions used for the stressed samples were as follows:

Hot-pressing stress: GDL samples were hot-pressed at 135 °C and 435 psi for 5 min;
Assembly stress: GDL samples were assembled in a cell with a bladder pressure of 200 psig for 30 min.

2.2. Alternative barriers investigation

Since it is unfeasible to separate the GDL intact from the aged MEA due to the adhesive property of PTFE and/or carbon particle, different barriers without catalyst have been employed for GDL stability and degradation research in this study. The barrier was sandwiched between the anode and cathode GDL and no catalyst was used in the degradation testing to avoid the impact of carbon particles, Nafion® ionomer and Pt from the catalyst layer. Nafion® membrane, a combination of the Nafion® membrane and a polyimide film, and one novel barrier were investigated, with the latter barrier eventually being utilized.

Nafion® 117 membrane was initially utilized as the barrier to separate anode and cathode GDLs. As shown in Fig. 1a and b, after an aging test of 200 h under high dynamic potential condition, portions of the MPL on the membrane-facing side of the GDL samples bonded to the Nafion membrane after its removal. Due to the adhesion, it was impossible to successfully remove the degraded GDL intact. This is also the reason that most research studies have focused on the ex situ analysis of GDL degradation.

The second barrier included covering a sample of Nafion® 112 membrane with a perforated polyimide film, as shown in Fig. 2a. The Nafion membrane was slightly larger than the active area, while the polyimide film was the same size as the flow field plates. The polyimide film was chosen due to its superior thermal and chemical stability. In order to allow water transport through the barrier, the active area where the GDL samples were located was perforated by needle at a hole density of 16 holes cm^{-2}. After approximately 70 h of aging under the dynamic potential condition, it shows that the degraded GDL samples were easier to peel off from the bar-

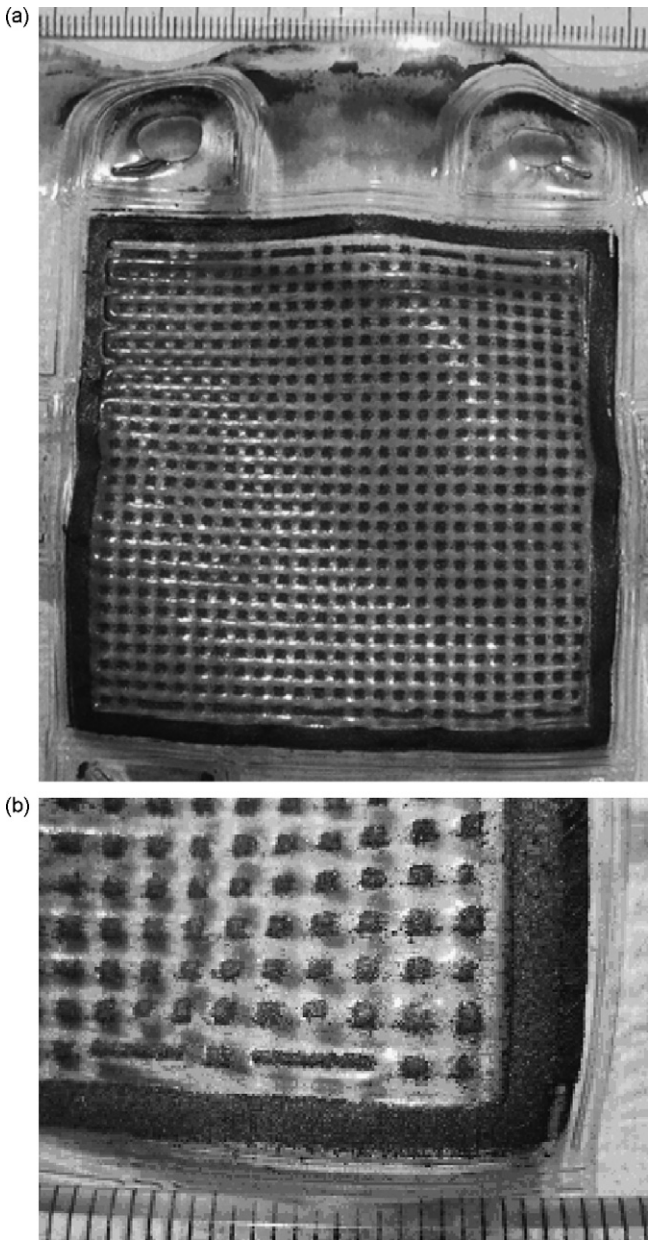

Fig. 1. Nafion® 117 membrane barrier after utilization as a barrier in a degradation test (a); partial enlarged view of the membrane (b).

rier, compared with those attached to the first barrier. However, as shown in Fig. 2b, slight marks from the MPL of the GDLs were left on the Nafion membrane through the perforation in the polyimide film, a consequence of the membrane swelling that occurs in the saturated condition.

The third barrier test involved hot-pressing as-received GDL samples to a Nafion® 112 membrane repeatedly at 130 °C and 150 psi for 5 min each time until a layer of MPL had transferred to the membrane forming a sacrificial MPL layer. The change of the normalized Nafion/MPL weight with the number of hot-presses is shown in Fig. 3. The Nafion/MPL weight increases significantly at the first three hot-presses due to the adhesion of the MPL from the GDL to the membrane. As shown in Fig. 3, there is almost no change in the Nafion/MPL weight after the fourth hot-pressing procedure. The major advantage of this MPL is to help prevent further bonding between the Nafion and the GDL samples, which are used for the characterization as well as performance tests. Due to the porous nature of the sacrificial MPL, it was also expected that the

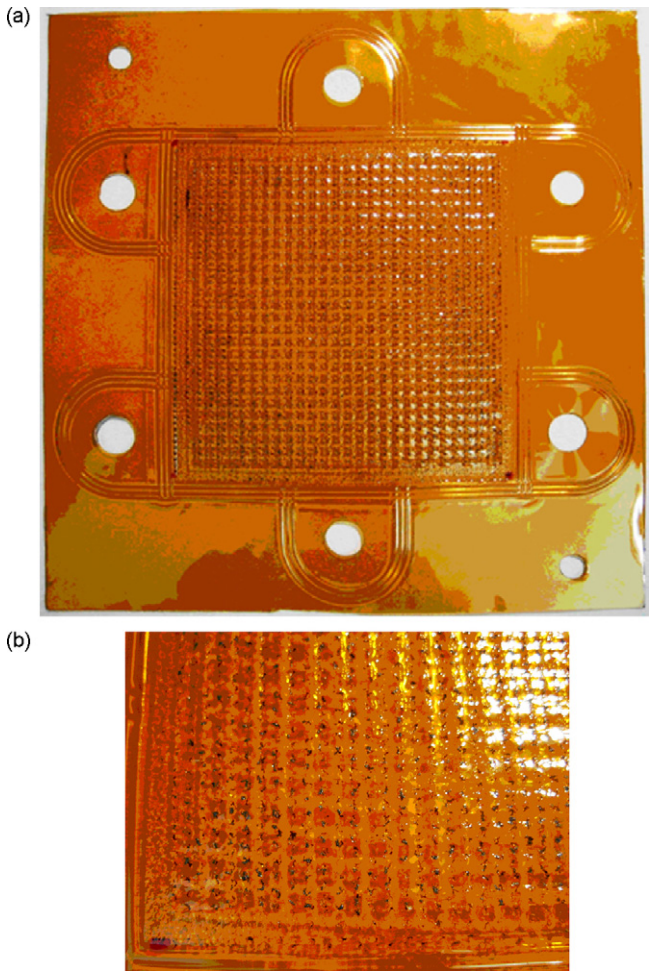

Fig. 2. Nafion® 112 membrane with a perforated polyimide film after utilization as a barrier in a degradation test (a); partial enlarged view of the barrier (b).

Nafion/MPL barrier would provide a better ionic connection. The polyimide film with silicon adhesive on one side was used as the sub-gasket to protect the edges of the Nafion membrane, leaving an active area of 50 cm^2. The Nafion/MPL/polyimide barrier that was utilized in the degradation tests consisted of a sheet of Nafion 112 membrane with a polyimide frame and an active area coated with MPLs on both sides applied after four hot-pressing procedures.

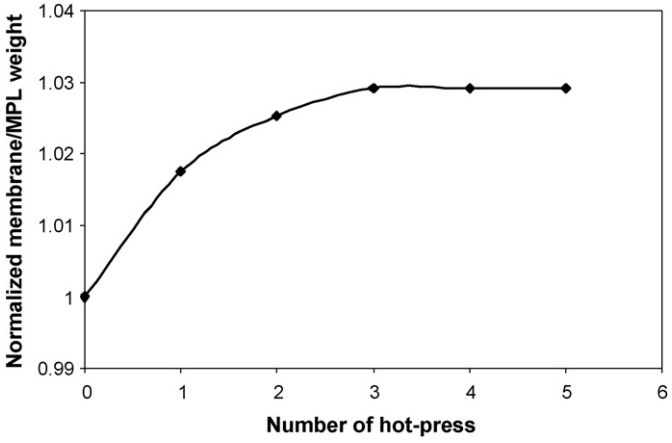

Fig. 3. Change of the normalized membrane/MPL weight with the number of hot-presses.

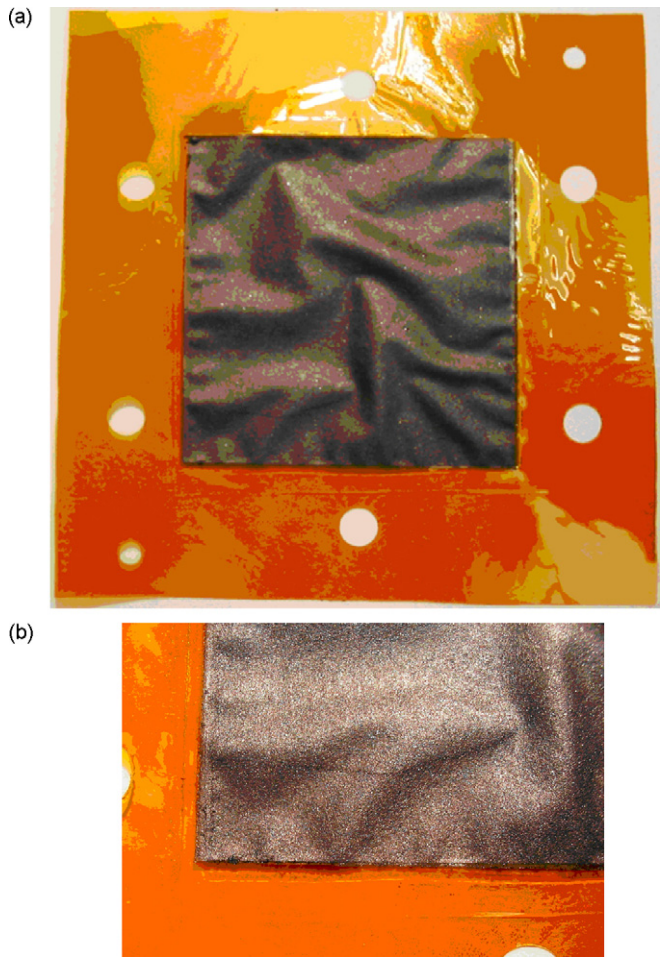

Fig. 4. Polyimide/Nafion/MPL barrier utilized in degradation testing (a); partial enlarged view of the barrier (b).

After 200 h of degradation testing, the final Nafion/MPL/polyimide barrier is shown in Fig. 4a and b, and no obvious changes in appearance or mass can be detected.

2.3. Post-characterization of degraded samples

Once the degradation phase was completed, the three sets of 50 cm^2 GDL samples were divided for further characterization. For every degraded GDL sample, two GDL test pieces, each with an area of 5 cm^2, were cut from the areas of reactant inlet and outlet respectively for performance and relatively humidity sensitivity tests. Two round GDL test pieces with an area of 2 cm^2 were cut from specific locations for through-plane electrical resistivity measurements, and the remainder was utilized for porosity measurement.

2.3.1. Performance and relative humidity (RH) sensitivity

The performance and RH sensitivity tests of the degraded GDL samples were conducted with a Medusa™ RD test station (Model 100 W, Teledyne Energy Systems, Inc., USA). For the fuel cell hardware, commercial hardware (Teledyne Energy Systems, Inc.) consisting of POCO graphite plates with triple parallel serpentine flow fields for both the anode and cathode were utilized. The active area of the hardware was 5 cm^2 and a co-flow configuration for hydrogen and air was employed in the experiments. To measure and compare the change of GDL samples before/after aging, all experiments were performed using Gore PRIMEA® Series 55 catalyst coated membrane (CCM) with a dry membrane thickness of 25 μm and a platinum loading of 0.4 mg cm^{-2} for both the anode and cathode.

In performance tests, the cell temperature was kept at 60 °C with hydrogen and air humidified at 60 and 50 °C, respectively. The cell was controlled under ambient backpressure and the stoichiometric coefficients for hydrogen and air were 1.5 and 3.0, respectively. RH sensitivity analysis, referred to as an RH fingerprint test, is a technique that has been utilized by Los Alamos National Laboratory (LANL) for characterizing GDL degradation [17]. The technique examines the response of cell performance to changes in the relative humidity of the reactant gases. In the RH sensitivity tests, the cell temperature was held at 60 °C while the humidification temperatures of the hydrogen and air were changed simultaneously in the range of 30–80 °C. The in situ current interrupt technique was utilized to measure internal cell ohmic resistance during the experiments [18]. A constant voltage of 0.6 V was chosen and the variations in current, as well as current interrupt cell resistance, with reactant humidification temperatures were monitored.

2.3.2. Electrical resistivity

The through-plane electrical resistivity of the as-received and degraded GDL samples was measured. The 2 cm^2 round GDL test piece, which was cut from a specific area of the GDL sample, was sandwiched between two gold-coated copper plates and compressed under a pressure of 175 psi. A current (I) of 4.0 A was applied with an Agilent E3510A DC power supply and the resulting voltage drop between two gold-coated plates (ΔV) was measured with a Fluke 87 True RMS multimeter. The through-plane electrical resistance (R) was described by:

$$R = \frac{\Delta V}{I} = \frac{\rho \cdot L}{A} \quad (1)$$

where ρ was through-plane electrical resistivity, A was the area of the GDL sample and L was the thickness of the GDL test piece under 175 psi compressive load. Thus, the through-plane electrical resistivity can be determined by re-arranging Eq. (1):

$$\rho = \frac{\Delta V}{I}\frac{A}{L} \quad (2)$$

2.3.3. Porosity

The porosity data for the GDL samples was obtained using an Auto Pore IV 9500 V1.05 mercury intrusion porosimeter (Micromeritics Instrument Corp., USA). The applied pressure for injection of mercury into the sample is inversely proportional to the pore radius in the sample in accordance with the Washburn equation and consequently, the pore size distribution can be calculated from mercury porosimetry data.

3. Results and discussion

3.1. Change in through-plane resistivity

Fig. 5a shows the through-plane electrical resistivity of the as-received and mechanically stressed GDLs prior to degradation testing. The resistivity of the as-received anode and cathode GDL samples is 0.40 and 0.62 Ω cm, respectively. After mechanical treatment, the resistivity of the stressed GDL samples is higher than that of as-received ones, especially for the cathode GDL samples, whose increased electrical resistivity is more significant (see Fig. 5a). For the hot-press stressed cathode, the through-plane electrical resistivity is 0.78 Ω cm, while the resistivity of the assembly stressed cathode is 0.85 Ω cm, which is approximately 38% higher than that of as-received cathode. This increase in resistance is likely caused by a weakening of the GDL structure during mechanical treatment, such as the carbon fiber breakage at the land/channel edge or the

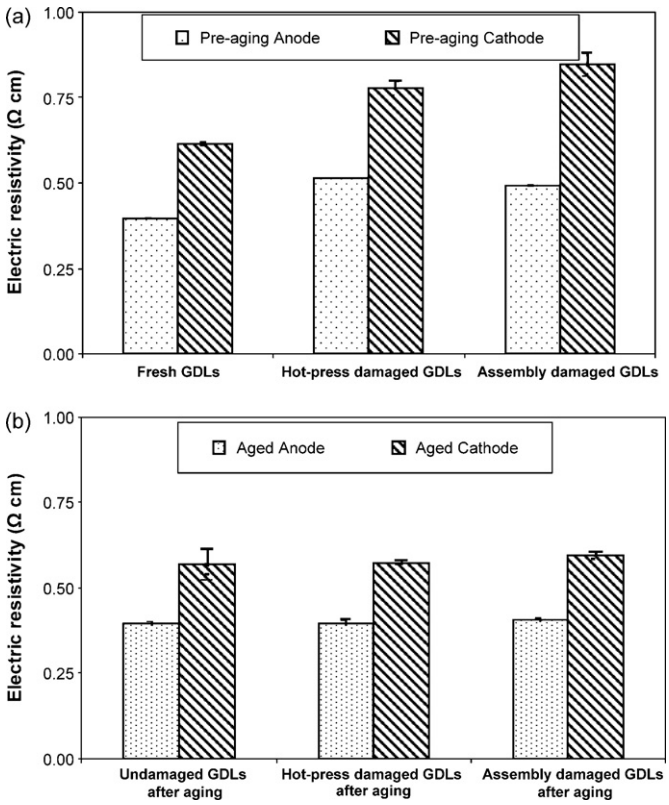

Fig. 5. Through-plane electrical resistivity of the as-received GDL and mechanically stressed GDL test pieces before aging (a) and after aging (b).

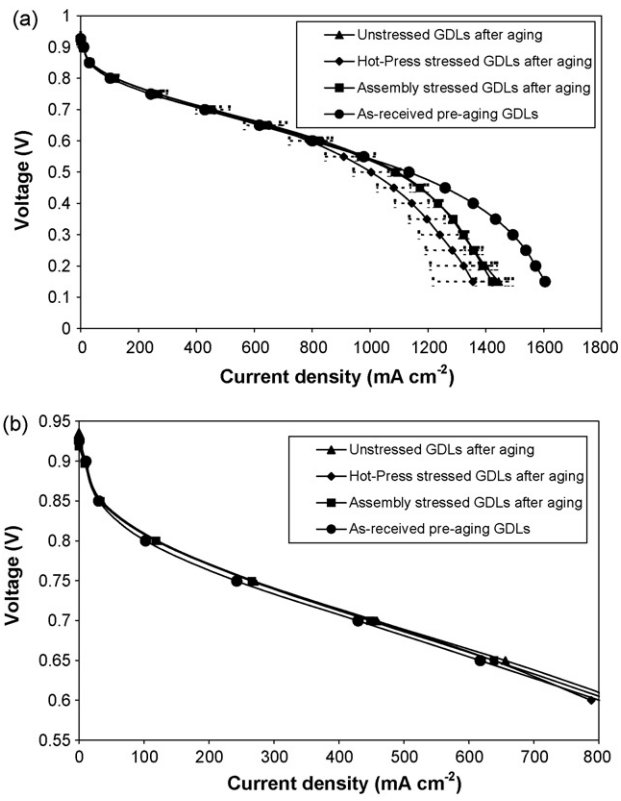

Fig. 6. 5 cm^2 single-cell performance comparison between the as-received and aged GDL sample sets (a) and its partial enlarged diagram without error bars (b).

structure collapse of carbon particles and PTFE in the MPL, which negatively impacts the through-plane electrical resistivity.

The through-plane electrical resistivity of the aged GDLs, including unstressed, hot-press stressed and assembly stressed samples, is shown in Fig. 5b. After aging under accelerated conditions of elevated temperature and elevated flow rate, the electrical resistivity of the unstressed anode and cathode GDL samples is slightly lower than that of the as-received ones, and it becomes 0.40 and 0.57 Ω cm for aged anode and cathode, respectively. However, it is worth noting that the resistivity of the hot-press and assembly stressed GDL samples drops dramatically. As shown in Fig. 5b, the electrical resistivity of the aged GDLs with mechanical treatment is very close to that of unstressed GDL anode and cathode. The decrease in resistivity for all GDL samples is likely attributed to the material loss, e.g., nonconductive PTFE loss from the substrate or MPL during aging at elevated temperature and elevated flow rates. In the case of hot-press and assembly stressed GDLs, this phenomenon becomes pronounced due to the weakened structure during the mechanical treatment, which would likely cause more GDL material loss during aging.

3.2. Change in performance and RH sensitivity

As-received and aged GDL samples were assembled with fresh CCM samples to test the effect of GDL aging on fuel cell performance. Fig. 6a and b shows the single-cell polarization curves with the as-received and aged GDL sample sets, which were obtained by recording the current change as a function of cell potential. As for Fig. 6b, it is a partial enlarged diagram of Fig. 6a in the range of 0–800 mA cm^{-2}. Since all performance experiments were conducted using fresh Gore PRIMEA Series 55 CCM, the activation overpotentials due to the sluggish kinetics of oxygen reduction reaction at low current densities should be relatively uniform. Consequently, for all the GDL sample sets, there is almost no difference in performance in low current density range of 0–50 mA cm^{-2}, as shown in Fig. 6b. At intermediate current densities from around 50 to 700 mA cm^{-2}, the cell's performance with aged GDL samples are very close and slightly higher than that with as-received pre-aging GDLs. In this region, ohmic overpotential is the dominant cause of voltage loss and the cell potential decreases nearly linearly with current density. As mentioned above, the nonconductive PTFE loss during aging can lead to the decrease in through-plane electrical resistance of degraded GDLs. Compared with as-received pre-aging GDL, another contribution to the ohmic overpotential reduction is the drop-off of contact resistances at the GDL/CCM and GDL/plate interfaces due to the nonconductive PTFE loss of degraded GDLs during performance experiments. At high current densities, the mass transport losses of the reactants for the cells with the three sets of aged GDL samples are significantly more drastic than that with as-received GDLs, as demonstrated in Fig. 6a.

In order to analyse GDL hydrophobicity loss, an RH sensitivity analysis of the as-received and degraded GDL samples was also conducted with the Teledyne single cell hardware, the results of which are shown in Fig. 7. The cell operating temperature was maintained at 60 °C while the humidification temperatures of the hydrogen and air were increased from 30 or 35 to 80 °C. At low humidification temperatures (less than 40 °C) the reactant gases were under-saturated prior to their introduction into the cell. Furthermore, the cell was operated at relatively high potential of 0.6 V, which likely causes the amount of water removed from the cell to be higher than the amount of water generated by the reaction plus the water introduced. In this case, water management becomes a major challenge, resulting in membrane drying and inferior performance. As a result, for the tests with either as-received or aged GDL samples, current interrupt resistances for the case of low reactant

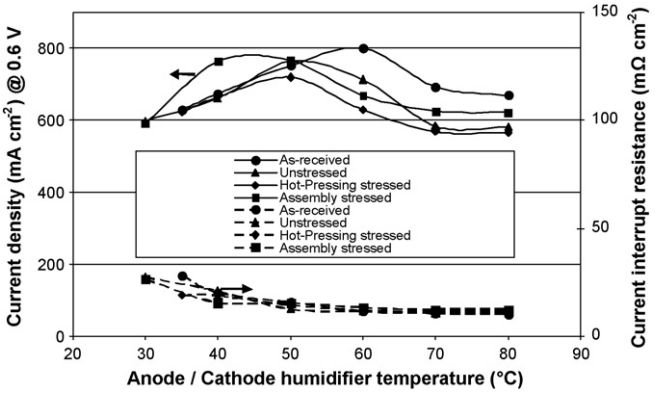

Fig. 7. Comparison of RH sensitivity and current interrupt resistance between the as-received and aged GDL sample sets.

humidification are relatively high due to the poor proton conductivity of the drier membrane.

With increasing reactant humidified temperatures, more water is introduced into the cell, which can mitigate membrane dryness and increase the hydration of the ionomer in the catalyst layer. Therefore, the ohmic resistance of the cell decreases and correspondingly, the cell performance increases with increasing humidification temperature until a maximum performance is reached. For the cell with as-received GDLs, the maximum performance is achieved when the humidification temperature is 60 °C. However, for the cells with aged GDL sample sets, including unstressed, hot-press stressed and assembly stressed GDLs, the maximum performances are obtained at lower humidification temperatures of approximately 52, 49 and 45 °C, respectively. When the cell exhibits the maximum performance, the desirable water balance is realized in the cell, which means the membrane remains well hydrated and at the same time no liquid water accumulates in the cell. The difference in RH sensitivities of as-received and degraded GDL samples is closely related to the change of their hydrophobic/hydrophilic properties before/after accelerated degradation [17]. In addition, the change in the pore structure of the degraded GDL samples could give rise to this behaviour; however, as described below in Section 3.3, no significant change can be observed in their pore size distributions. Thus one can discount changes in pore structure as the cause of the RH sensitivity variations observed. Compared with as-received pre-aging GDLs, the optimal humidification temperatures of the three sets of degraded GDL samples drops dramatically, most likely indicating hydrophobic material loss during aging, which is in agreement with the abovementioned results of through-plane resistance. Clearly, among the three degraded GDL sample sets, the assembly stressed GDL sample set shows the most hydrophobicity loss due to the weakened structure before aging, while the unstressed GDL sample set demonstrates the least hydrophobicity loss. It is noteworthy that the maximum current density of the hot-press stressed GDL sample set is reduced significantly in addition to the decrease in the optimal humidifier temperature. This reduction in maximum current density for the hot-press stressed GDL sample set demonstrates clearly the weakened capacities of water management and reactants transport, which can be attributed to the severe structure damage during the mechanical overstress, as well as material loss and porosity change during aging.

For as-received and all degraded GDL sample sets, the cell performance apparently decreases when reactant humidification temperatures increase beyond their optimal values, while the cell ohmic resistance remains at an almost constant value, as shown in Fig. 7. This can be explained as an indication of excess liquid water clogging the electrodes and/or flow channels, leading to a flooding

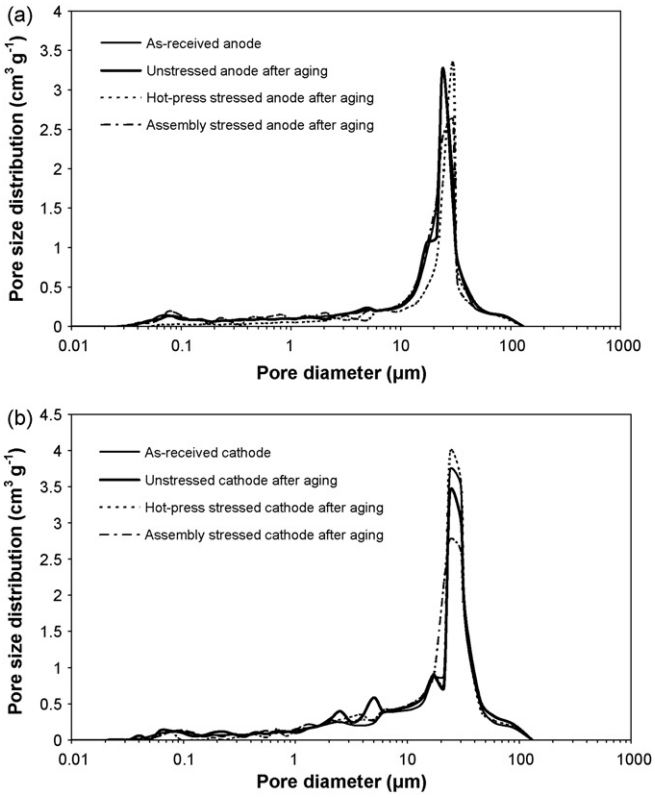

Fig. 8. Pore size distribution comparison between the as-received and aged anode (a) and the as-received and aged cathode (b).

problem at high humidification temperatures. The decrease in optimal humidification temperature for aged GDLs implies a reduction in water management, which may cause many critical issues when the cell is operated under relatively high RH condition, such as flooding and inactivity of the catalyst layer, and/or limited oxygen permeability through the GDL to the catalytic sites, and eventually be a detriment to fuel cell performance and durability.

3.3. Change in pore size distribution and total porosity

Mercury intrusion porosimetry measurements were conducted to determine the pore size distribution changes in the GDL samples. As shown in Fig. 8a and b, for the as-received and degraded TORAY® TGPH-060 anode and cathode GDLs with MPLs, only large macropores of 10–100 μm radius can be found and no other pores are present. With regard to the total porosity of all aged anode GDL samples, no obvious change is observed except for the hot-press stressed anode from Table 1, due to the relatively low hydrogen flow rate during aging. However, a little increase in total porosity can be noticed for all aged cathode GDL samples, which can be attributed to the material loss during aging. The function of PTFE is to impart a hydrophobic nature to the GDL and also provide bond-

Table 1
Total porosity of as-received and aged GDL samples.

GDL samples	Total porosity (%)
As-received pre-aging anode	64
Unstressed anode after aging	62
Hot-press stressed anode after aging	44
Assembly stressed anode after aging	64
As-received pre-aging cathode	62
Unstressed cathode after aging	71
Hot-press stressed cathode after aging	65
Assembly stressed cathode after aging	67

ing to the carbon particles, which means that the PTFE loss might likely cause the increase in porosity of the aged GDL samples. The reason that the total porosity of the hot-press stressed cathode is much higher than that of the anode may be ascribed to more severe material loss on cathode side. For both anode and cathode GDL samples, the hot-pressing treatment at 435 psi and 135 °C most likely collapses the structure of carbon particles and PTFE in the MPL, and simultaneously results in the dramatic decrease in the total porosity at the same time. The significant PTFE and carbon particles loss might further weaken the GDL structure and increase the total porosity of the hot-press stressed and aged cathode GDL sample. While for anode GDL, the less PTFE loading and low hydrogen flow rate may cause less material loss and unobvious porosity change. It can be concluded that mechanical treatment of hot-pressing stress or assembly stress weakens GDL structure and accelerates its degradation. For the cell with the degraded GDL samples, including unstressed, hot-press stressed and assembly stressed GDL sets, the mass transport limitations at high current densities are mainly caused by the material loss in GDLs during aging, especially loss of the hydrophobic PTFE.

4. Conclusions

Three different barriers were explored, including a Nafion® membrane, a Nafion® membrane covered with a perforated polyimide film and Nafion® coated with sacrificial MPLs on both sides and a polyimide border. After the barriers were evaluated on their ability to isolate GDL degradation and their similarity to a fuel cell environment, the last barrier was chosen in our GDL degradation studies. The barrier was sandwiched between the anode and cathode GDLs and no catalyst was used in the degradation testing. For comparison, three sets of GDL samples were used simultaneously during the degradation testing, including one as-received unstressed GDL set, and two GDL sets stressed according to a simulation of excessive hot-press and assembly pressure prior to degradation. After 200 h accelerated degradation, an obvious decrease in through-plane resistivity of degraded GDL samples was observed, especially for two sets of mechanically stressed GDL samples. The degraded GDL samples exhibited less-hydrophobic characteristics, resulting in remarkable mass transport losses during the polarization curve measurements. The experimental results suggested that material loss, especially nonconductive PTFE loss, is the major mechanism of GDL degradation in an aging experiment. While for hot-press and assembly stressed GDLs, the excessive mechanical damage will weaken GDL structure, cause changes in the GDL characteristics and consequently accelerate the material loss in the GDL during aging.

Further work is still needed to measure and distinguish quantitatively the material loss from the substrate and MPL, respectively. To this end, for example, a plain GDL substrate with MPL or a hydrophobic-treated substrate without MPL can be employed in the degradation tests. From the viewpoint of practical applications of fuel cell technology, the accelerated degradation test results should correlate to real world degradation and the statistical accelerated lifetime testing model [19] will be utilized in our further research. An investigation of the effects of different accelerated conditions, such as a combination of elevated temperature, elevated flow rate and dynamic electrical potential, on PEM fuel cell degradation will be reported soon.

Acknowledgements

The authors acknowledge the Ballard-NRC IFCI Joint Research Program, NRC-MOST Joint Research Program, BCIC's ICSD Program and NRC-Helmholtz Joint Research Program for the financial support.

References

[1] M.V. Williams, H.R. Kunz, J.M. Fenton, J. Electrochem. Soc. 151 (2004) A1617–A1627.
[2] H. Nakajima, T. Konomi, T. Kitahara, J. Power Sources 171 (2007) 457–463.
[3] G. Lin, T. Van Nguyen, J. Electrochem. Soc. 152 (2005) A1942–A1948.
[4] U. Pasaogullari, C.Y. Wang, K.S. Chen, J. Electrochem. Soc. 152 (2005) A1574–A1582.
[5] G.G. Park, Y.J. Sohn, T.H. Yang, Y.G. Yoon, W.Y. Lee, C.S. Kim, J. Power Sources 131 (2004) 182–187.
[6] H.K. Atiyeh, K. Karan, B. Peppley, A. Phoenix, E. Halliop, J. Pharoah, J. Power Sources 170 (2007) 111–121.
[7] J. St-Pierre, N. Jia, J. New Mater. Electrochem. Syst. 5 (2002) 263–271.
[8] M. Oszcipok, D. Riemann, U. Kronenwett, M. Kreideweis, M. Zedda, J. Power Sources 145 (2005) 407–415.
[9] J.W. Frisk, M.T. Hicks, R.T. Atanasoski, W.M. Boand, A.K. Schmoeckel, M.J. Kurkowski, Fuel Cell Seminar San Antonio, TX, USA (November 1–5, 2004), 2004.
[10] R. Borup, J. Davey, D. Wood, F. Garzon, M. Inbody, D. Guidry, PEM fuel cell durability, DOE Hydrogen Program, FY 2004 Progress Report.
[11] K.H. Kangasniemi, D.A. Condit, T.D. Jarvi, J. Electrochem. Soc. 151 (2004) E125–E132.
[12] C. Lee, W. Mérida, J. Power Sources 164 (2007) 141–153.
[13] M. Schulze, N. Wagner, T. Kaz, K.A. Friedrich, Electrochim. Acta 52 (2007) 2328–2336.
[14] S. Srinivasan, B. Kirby, in: S. Srinivasan (Ed.), Fuel Cells: From Fundamentals to Applications, Springer Science + Business Media, 2006, pp. 441–573.
[15] J.F. Wu, S. Galli, I. Lagana, A. Pozio, G. Monteleone, X.Z. Yuan, J.J. Martin, H.J. Wang, J. Power Sources 188 (2009) 199–204.
[16] J.F. Wu, X.Z. Yuan, J.J. Martin, H.J. Wang, D.J. Yang, J.L. Qiao, J.X. Ma, J. Power Sources 195 (2010) 1171–1176.
[17] R.L. Borup, J.R. Davey, F.H. Garzon, D.L. Wood, P.M. Welch, K. More, ECS Trans. 3 (2006) 879–886.
[18] http://www.scribner.com/890e-multi-range-electronic-test-loads.html (accessed September 2009).
[19] J.F. Wu, X.Z. Yuan, J.J. Martin, H.J. Wang, in: J. Garche (Ed.), Encyclopedia of Electrochemical Power Sources, vol. 2, Elsevier, Amsterdam, 2009, pp. 848–867.